The Journal of Chemical Physics

Cryo infrared spectroscopy of N_2 adsorption onto bimetallic rhodium–iron clusters in isolation

Cite as: J. Chem. Phys. **156**, 014302 (2022); https://doi.org/10.1063/5.0075289
Submitted: 14 October 2021 • Accepted: 18 November 2021 • Accepted Manuscript Online: 23 November 2021 • Published Online: 04 January 2022

Matthias P. Klein, Amelie A. Ehrhard, Maximilian E. Huber, et al.

openaccess
View Online
Export Citation
CrossMark

ARTICLES YOU MAY BE INTERESTED IN

Cryo spectroscopy of N_2 on cationic iron clusters
The Journal of Chemical Physics **155**, 244305 (2021); https://doi.org/10.1063/5.0064966

Kinetics of stepwise nitrogen adsorption by size-selected iron cluster cations: Evidence for size-dependent nitrogen phobia
The Journal of Chemical Physics **155**, 244306 (2021); https://doi.org/10.1063/5.0064965

Noble-gas compounds: A general procedure of bonding analysis
The Journal of Chemical Physics **156**, 014104 (2022); https://doi.org/10.1063/5.0077119

AIP Publishing

© 2022 Author(s).

The Journal of Chemical Physics ARTICLE scitation.org/journal/jcp

Cryo infrared spectroscopy of N_2 adsorption onto bimetallic rhodium–iron clusters in isolation

Cite as: J. Chem. Phys. 156, 014302 (2022); doi: 10.1063/5.0075289
Submitted: 14 October 2021 • Accepted: 18 November 2021 •
Published Online: 4 January 2022

View Online Export Citation CrossMark

Matthias P. Klein, Amelie A. Ehrhard,[a] Maximilian E. Huber, Annika Straßner, Daniela V. Fries, Sebastian Dillinger, Jennifer Mohrbach, and Gereon Niedner-Schatteburg[b]

AFFILIATIONS

Fachbereich Chemie and Forschungszentrum OPTIMAS, Technische Universität Kaiserslautern, 67663 Kaiserslautern, Germany

[a]**Present address:** Max-Planck-Institut für Polymerforschung, 55128 Mainz, Germany.
[b]**Author to whom correspondence should be addressed:** gns@chemie.uni-kl.de.
Permanent address: Gereon Niedner-Schatteburg, Erwin-Schrödinger-Straße 52, 67663 Kaiserslautern.

ABSTRACT

We investigated the N_2 adsorption behavior of bimetallic rhodium–iron cluster cations $[Rh_iFe_j(N_2)_m]^+$ by means of InfraRed MultiplePhotoDissociation (IR-MPD) spectroscopy in comparison with density functional theory (DFT) modeling. This approach allows us to refine our kinetic results [Ehrhard *et al.*, J. Chem. Phys. (in press)] to enhance our conclusions. We focus on a selection of cluster adsorbate complexes within the ranges of $i = j = 3$–8 and $m = 1$–10. For $i = j = 3, 4$, DFT suggests alloy structures in the case of $i = j = 4$ of high (D_{2d}) symmetry: Rh–Fe bonds are preferred instead of Fe–Fe bonds or Rh–Rh bonds. N_2 adsorption and IR-MPD studies reveal strong evidence for preferential adsorption to Rh sites and mere secondary adsorption to Fe. In some cases, we observe adsorption isomers. With the help of modeling the cluster adsorbate complex $[Rh_3Fe_3(N_2)_7]^+$, we find clear evidence that the position of IR bands allows for an element specific assignment of an adsorption site. We transfer these findings to the $[Rh_4Fe_4(N_2)_m]^+$ cluster adsorbate complex where the first four N_2 molecules are exclusively adsorbed to the Rh atoms. The spectra of the larger adsorbates reveal N_2 adsorption onto the Fe atoms. Thus, the spectroscopic findings are well interpreted for the smaller clusters in terms of computed structures, and both compare well to those of our accompanying kinetic study [Ehrhard *et al.*, J. Chem. Phys. (in press)]. In contrast to our previous studies of bare rhodium clusters, the present investigations do not provide any indication for a spin quench in $[Rh_iFe_j(N_2)_m]^+$ upon stepwise N_2 adsorption.

© 2022 Author(s). All article content, except where otherwise noted, is licensed under a Creative Commons Attribution (CC BY) license (http://creativecommons.org/licenses/by/4.0/). https://doi.org/10.1063/5.0075289

I. INTRODUCTION

Transition metal clusters may serve as model systems for elemental processes that are of relevance in the context of heterogeneous catalysis.[1,2] Such catalysts may consist of several metal components, either separated or as alloys, that contribute to the catalytic activity for various reactions:[3] In the automobile three way catalyst, a combination of precious metals catalyzes oxidation of hydrocarbons and reduction of CO and nitrous oxides.[4] The latter takes place on rhodium sites and effects the production of N_2 and CO_2.[5,6] Iron is well known as a catalyst for dinitrogen activation, especially in the Haber–Bosch process. In this case, N_2 activation is considered as the rate limiting step. In the course of activation, physisorption of N_2 is the precursor state.[7] Apart from this, the adsorption of N_2 onto surfaces to study the surface properties was an early research field.[8,9]

Surface studies also provided information about the binding states of N_2 on Fe surfaces: α-N_2 (side-on) and γ-N_2 (end-on) adsorption motifs were identified.[10] Upon adsorption onto rhodium surfaces, N_2 is polarized and the otherwise IR inactive N_2 stretching vibration becomes IR active.[11] Thus, chemisorbed and physisorbed N_2 species were identified where the physisorbed ones reveal no shift of the N_2 stretching vibration and are only very weakly bound (adsorption heat: 1.6 kcal/mol). The adsorption state and the adsorption site determine the stretching frequency. Recently, spectroscopic investigations of N_2 adsorption on zirconia supported Rh nanoparticles were used to investigate step-edge sites that are required to dissociate CO.[12] IR bands of N_2 adsorbed onto an oxidized or reduced Rh layer appear at 2293 or 2205 cm^{-1}, respectively. The π-backbonding effect could be instrumentalized to selectively adsorb N_2 onto exposed vanadium centers in a metal organic framework.[13]

Isolated transition metal clusters such as neutral Ru_n clusters also polarize and activate N_2 and make it accessible to infrared spectroscopy.[14] The vibrational bands were observed red shifted

with respect to the free N_2 vibration. For cases of N_2 adsorbed onto cobalt cluster cations, we found similar red shifts of the N_2 stretching frequencies.[15] The interaction between metal atoms at surfaces and adsorbates containing π-bonds can be explained in terms of the Blyholder model.[16] This model refers to the same σ-donor, π-acceptor synergism as the Dewar–Chatt–Duncanson model for coordination compounds.[17,18] The dependence of CO stretching frequencies on the number of metal atoms within the cluster can be explained by using the Fielickes charge dilution model.[19]

In addition, InfraRed MultiplePhotoDissociation (IR-MPD) spectra of CO and N_2 adsorbed onto a rhodium cation $[Rh(N_2/CO)_m^+]$ reveal a red shift of the N–N vibration and a blue shift of the CO vibration in the case of $m = 4$.[20] With the help of density functional theory (DFT) calculations, this result could be explained by a combination of σ-donation and electrostatic polarization of the ligand. The interaction of the non-polar N_2-molecule with the metal atom is much weaker than that of the isoelectronic but polar CO. In N_2, HOMO and LUMO are symmetrically shared by both atoms, and the HOMO–LUMO gap is considerable. In CO, HOMO and LUMO are mainly located on the carbon atom, which allows for a stronger bonding and back-bonding interaction with the metal atom. The HOMO–LUMO gap is significantly smaller than that of N_2.

Until now, we published cryo-spectroscopic investigations of N_2 adsorption on Co,[15] Ni,[21,22] Ru,[14,23] and Rh[24] clusters. A combination of IR studies with N_2 adsorption kinetics proved useful to investigate cluster surface morphologies and to discriminate *rough* and *smooth* cluster surfaces in the case of Ni.[21,22,25] IR-MPD spectroscopy of $[Rh_i(N_2)_m]^+$ clusters revealed coexisting isomers and a spin quench upon N_2 adsorption.[24] It is necessary to support the experimental work with theoretical models, but in the case of clusters, these often reach their limits.[26]

Rhodium–iron alloys were found to reveal interesting magnetic properties, such as transitions between antiferromagnetic and ferromagnetic states.[27–40] In particular, theoretical studies have been performed to determine structures and magnetism of neutral $[Rh_iFe_j]$ clusters and they provide a set of initial structures for our own modeling and a basis of comparison with obtained data.[41] In particular, for small clusters, Rh–Fe bonds are stronger than Fe–Fe and Rh–Rh bonds.[40] These differences diminish with an increase in the size of the cluster. The investigation of possible activation mediated by Fe atoms in mixed metal clusters is of interest for further catalyst development, and the N_2 stretching vibration may help to elucidate the cluster structure, in particular the distribution of metal atoms of the alloy or layered-type clusters.

Together with the accompanying kinetic paper **[AAE]**,[42] we present a combined spectroscopic and kinetic approach to investigate the N_2 adsorption steps and the cluster adsorbate complexes themselves. This approach has proven successful in the case of Ni clusters before.[22,25] To facilitate readability, we use the short notation (i,j,m) for the cluster adsorbate complexes $[Rh_iFe_j(N_2)_m]^+$. The kinetic study presents extensive adsorption kinetic data for all cluster adsorbate complexes (i,j,m) with $i = j$, $i = j + 1$, and $i + 1 = j$ for $i = 3, \ldots, 8$ and $j = 3, \ldots, 8$ in the range of $(3,3,m), \ldots, (8,8,m)$.

In our present study, we investigated a selection of cationic $[Rh_iFe_j(N_2)_m]^+$ cluster adsorbate complexes by means of infrared multiphotodissociation spectroscopy (IR-MPD). Single and maximum adsorption and special intermittent sizes are of special interest. We interpret the obtained spectra in conjunction with corresponding DFT calculations. We chose to select for investigation the equiatomic $[Rh_iFe_j(N_2)_m]^+$ clusters with single N_2 adsorption ($m = 1$) and intermittent and high coverages, where the high load cases do not necessarily represent the maximum adsorption limit as defined in **[AAE]**. We compare our recorded IR-MPD spectra to those of pure rhodium and iron clusters.[24,43] In the present study, we focused on N_2 adsorbates of the equiatomic (i,j,m) clusters, $i = j = 3, \ldots, 8$.

For a description of the chosen (i,j,m) nomenclature and for a detailed discussion of the adsorption kinetics, refer to the accompanying kinetics paper **[AAE]**[42] and to supplementary material S1 of Ref. 44.

II. EXPERIMENTAL METHODS AND COMPUTATIONAL APPROACH

In a customized 7 T Fourier Transform-Ion Cyclotron Resonance (FT-ICR)-mass spectrometer (Apex Ultra Bruker Daltonics), the metal clusters were produced and isolated. We let N_2 adsorb and performed InfraRed PhotoDissociation (IR-MPD) and mass analysis. The detailed construction and experimental procedure have been described elsewhere.[15,22,42] In short, the $[Rh_iFe_i]^+$ clusters were generated by laser vaporization from a RhFe-target (^{103}Rh:^{56}Fe stoichiometry 1:1, *MaTecK*) and mass selected by using a quadruple mass filter. The selected clusters are stored into a cryogenic hexapole ion trap, which is cooled to 26 K. The attachment of nitrogen is achieved by introducing N_2, and we maintain the requested constant pressure of about $2.2–3.2 \times 10^{-7}$ mbar N_2. We increase the pressure in the ion trap to roughly 3.0×10^{-6} mbar by adding helium gas to accomplish efficient trapping and cooling of the ions. The ions are stored for a variable time (0.0–3.0 s). Subsequently, the cluster ions are steered into the ICR-cell using various electrostatic ion lenses. Our ICR-cell of the so-called infinity-type[45] is cooled down to 10 K by using a closed cycle He cryostat to prevent heating of the clusters by black body radiation.

To study the N_2 adsorbates of the selected $[Rh_iFe_j]^+$ clusters within the ICR cell, we first isolate the metal cluster of interest in the quadrupole mass filter and afterward the cluster adsorbate complex of interest in the ICR cell and remove all other ions by correlated frequency sweeps and shots.

The number m of adsorbed N_2 on the cluster can be controlled by varying the storage time in the hexapole collision cell. The storage time can be increased until the number of N_2 adsorbed reaches a maximum limit, and at higher storage times, no further N_2 adsorption is observed, as is shown for $[Rh_3Fe_3]^+$ (Fig. 1). The $[Rh_3Fe_3]^+$ and $[Rh_4Fe_4]^+$ cluster can adsorb up to seven and eight N_2 molecules, respectively. We can observe an additional *intermittent adsorption limit* for some metal cluster cores, e.g., $[Rh_4Fe_4(N_2)_4]^+$. Here, the course of adsorption seems intermittent/interrupted, but it may continue with a lower adsorption rate. Detailed kinetic investigations have confirmed that this behavior correlates with a slower rate of additional N_2 adsorption above this intermittent limit **[AAE]**.[42] Upon closer inspection, the $[Rh_4Fe_4(N_2)_4]^+$ mass spectra further reveal but very weak adsorption peaks as discussed in the accompanying kinetic study. For the following spectroscopic investigations, we chose single N_2 adsorbed clusters and clusters at the *intermittent* and

© Author(s) 2022

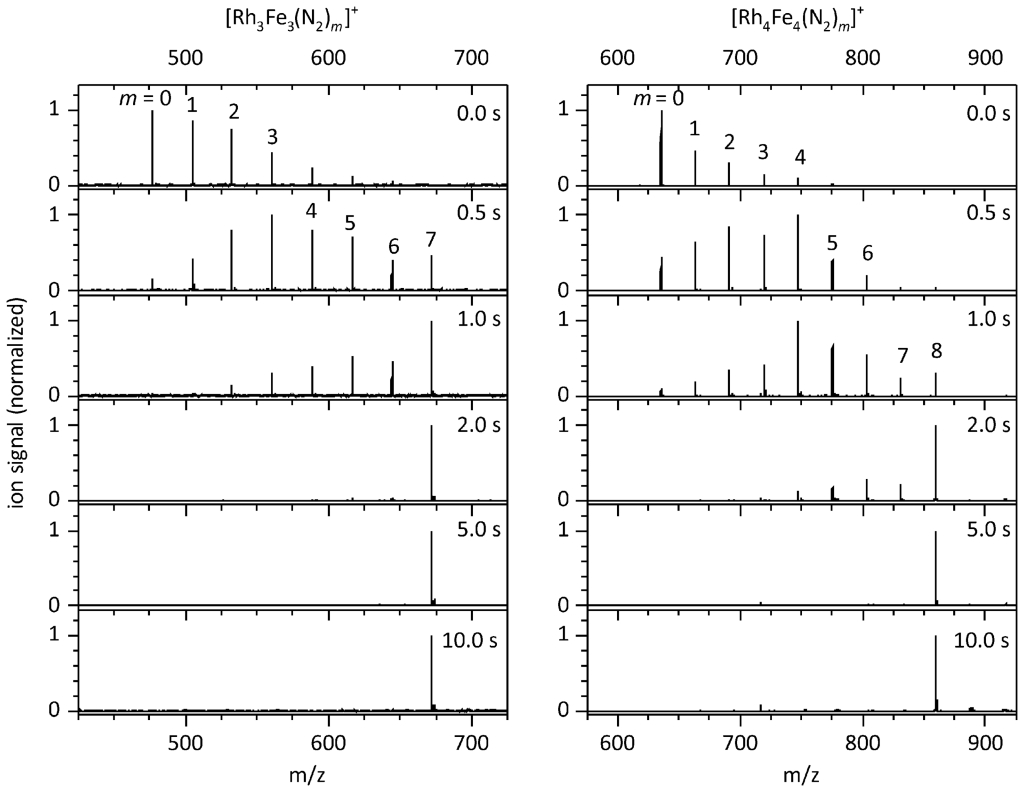

FIG. 1. FT-ICR mass spectra of $[Rh_3Fe_3]^+$ and $[Rh_4Fe_4]^+$ exposed to 2.8×10^{-7} mbar N_2 at a temperature of 26 K with various storage times in the cryogenic hexapole ion trap. $[Rh_3Fe_3]^+$ reveals a *smooth* adsorption behavior up to a limit of 7 N_2, whereas measurements on the $[Rh_4Fe_4]^+$ cluster show, in addition to an adsorption limit of 8 N_2, an *intermittent* limit of 4 N_2, i.e., after a distinct number of N_2 is adsorbed, additional adsorption of N_2 happens with a slower rate (confirmed by detailed kinetic investigations done by **[AAE]**[42]).

maximum adsorption limit. The adsorption limits are given in **[AAE]**,[42] Fig. 2.

A tunable IR laser system is coupled to the ICR cell to affect fragmentation of the stored ions. This laser is a potassium titanyl phosphate potassium titanyl phosphate/potassium titanyl arsenate (KTP/KTA) optical parametric oscillator/amplifier (OPO/A, *LaserVision*) system pumped by a pulsed 10 Hz injection seeded Nd:YAG laser (PL8000, *Continuum*) followed by an $AgGaSe_2$ crystal to generate the difference frequency (DF) between signal and idler waves.[46] This method can generate IR radiation in the range of 1200–2400 cm^{-1}. Each trapped and isolated package of ions is irradiated by 7–10 laser pulses to yield a sufficient number of fragment ions. A typical pulse energy spectrum is given in Fig. S1. The IR spectra were recorded as a series of mass spectra while continuously scanning the IR wavelength. We evaluated the IR-MPD signal as $\Sigma_n F_n/(\Sigma_n F_n + \Sigma_x P_x)$, where F_n and P_x indicate fragment and the parent ion signals, respectively. An IR-MPD spectrum as depicted in this work arises out of plot of the fragmentation efficiency as a function of laser frequency. We employed the IR-MPD spectroscopy in the 2140–2350 cm^{-1} range on the $[Rh_iFe_j(N_2)_m]^+$ species ($i = j = 3, \ldots, 8$ and $m = 1, \ldots, 10$). In this range, we expected the end-on N_2 stretching frequencies of the species. We expanded this range to 1160–2400 cm^{-1} in selected cases to check for non-end-on N_2 ligands. The N–N stretching bands of side-on adsorbed N_2 on various metal surfaces have been reported in the range of 1220–1590 cm^{-1} before.[47–52] We observed the band of side-on adsorbed N_2 on a Ta_4^+ cluster between 1443 and 1475 cm^{-1}.[53]

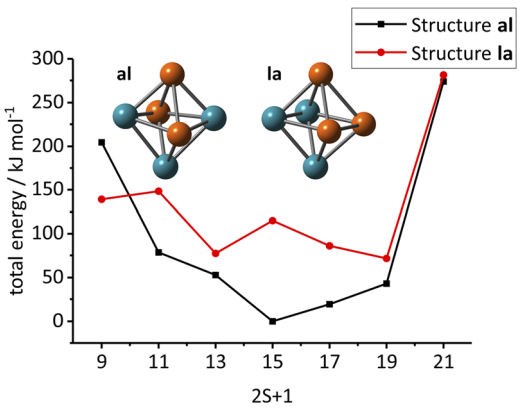

FIG. 2. Total energies of alloy-like $[Rh_3Fe_3]^+$ clusters (black squares) and of layered $[Rh_3Fe_3]^+$ clusters (red circles) as a function of spin multiplicity 2S + 1 relative to the 15tet of structure **(al)**. The insets display the two possible isomers in a near octahedral geometry (see the text for details; Fe: orange and Rh: turquoise).

© Author(s) 2022

For all complexes, the loss of the N_2 was the only observed fragmentation channel.

Geometry optimizations and vibrational analysis were performed by using the Gaussian 09 package[54] at the PBE0/ECP(Rh, Fe); cc-pVTZ(N) level of theory[55,56] as proven suitable for cobalt, nickel, and rhodium clusters.[15,21,22,24,44] We utilize Stuttgart RSC 1997 ECP(Rh) basis sets of double zeta quality.[57] We had to tolerate relaxed SCF convergence criteria of 10^{-5} (as compared to 10^{-8} in "standard" DFT calculations) to achieve SCF convergence.

III. RESULTS AND DISCUSSION

A. The computed structures and spin states of bare $[Rh_3Fe_3]^+$ and $[Rh_4Fe_4]^+$ clusters

We take as a starting point for our studies of bimetallic cluster adsorbate complexes $[Rh_iFe_j(N_2)_m]^+$, abbreviated as (i,j,m), the modeling of the minimum structures of the bare (3,3,0) and (4,4,0) clusters. The optimization toward a minimum energy structure is more involved for bimetallic clusters than for monometallic clusters: One needs to take into account several mixing topologies, which imply various topologic isomers.

The Rh_3Fe_3 cluster was found to assume an octahedral structure.[41] We took these findings as a basis for our calculations on the cationic $[Rh_3Fe_3]^+$ cluster. Within the octahedral geometry, there are exactly two possible distributions of 3 + 3 equivalent atoms: an intermixed "alloy" structure **(al)** and a segregated "layered" structure **(la)**. Pairwise permutation of any two non-equivalent atoms would interconvert these two isomers into each other (cf. insets of Fig. 2). Within the two possible octahedral isomers, the rhodium and iron atoms find themselves to form two alternative triangular arrangements, respectively (Fig. 2). These triangles are perpendicularly oriented to each other in the alloy-like structure **(al)** (meridional) and are parallel to each other in the layered structure **(la)** (facial).

In order to model such conceivable isomers, we had to explore their possible spin multiplicities in parallel. It showed that both isomers are stable in all multiplicities explored (2S + 1 = 9, . . ., 21) and that their geometries do relax to a minor extent by some symmetry lowering. The alloy structure **(al)** is most stable when in a 15tet. This value fits well to the average spin moment per atom ($\overline{\mu}_N = 2.50\mu_B$ of the neutral cluster 16tet) calculated by Mokkath and Pastor for structure **(al)**.[41] All of **(al)**'s multiplet states are more stable than those of the layered structure **(la)**—but the 9tet. The most favorable layered multiplet, the 19tet of **(la)**, is 72 kJ mol^{-1} less stable than the most favorable alloy multiplet, which is the 15tet of **(al)**.

We compare the atomic distances to the next neighbors of each atom in the previously shown structures **(al)** and **(la)** with the bulk values and the previously calculated neutral cluster distances[41] (Tables I, S1, and S2). Our calculated $[Rh_3Fe_3]^+$ cluster values come closer to the ones known from crystal data. The PW91 functional used by Mokkath *et al.*[41] overbinds the Rh–Rh and the Rh–Fe distances in an **(la)**-type cluster and yields longer Fe–Fe contacts, compared to this work. The range of Rh–Fe bond length in structure **(la)** reflects that there are two different coordination geometries for each element, and thus, the symmetry is lower than in structure **(al)**. Structure **(al)** provides eight Rh–Fe bonds, and structure **(la)** provides only six Rh–Fe bonds at the expense of additional Fe–Fe and Rh–Rh interaction.

TABLE I. Calculated atomic distances (in Å) of nearest neighbors within the two $[Rh_3Fe_3]^+$ cluster isomers **(al)** and **(la)** (15tet) in comparison with sums of atomic radii, with experimental data, and with calculations on an **(al)**-like structure.

	Sums of atomic radii		PW91[a]	PBE0[b]	PBE0[b]
Species	Dimer	Bulk	**(al)**	**(al)**	**(la)**
Rh–Rh	Theo. 2.21[a] Theo. 2.27[d] Exp. 2.3855[e] Exp. 2.28[f]	2.69[c]	2.61	2.737	2.725
Rh–Fe		2.586[c] 2.581[h]	2.38	2.643–2.666	2.65
Fe–Fe	Exp. 2.198(2) –2.2318(8)[g]	αFe 2.482[c]	2.62	2.580	2.584

[a]Reference 41.
[b]This work.
[c]Reference 62. Distance of the next neighbors in the fcc crystal; lattice parameter a = 3.8032 Å.
[d]Reference 58.
[e]Reference 59.
[f]Reference 60.
[g]Reference 61.
[h]Reference 63.

We started our survey for $[Rh_4Fe_4]^+$ minimum structures with bicapped octahedral structures **(b)**,[41] and we added cubic **(a)** and quadratic antiprismatic **(c)** and **(d)** structures, inspired by earlier investigations of pure Rh clusters by Harding *et al.*[64] In all these cases, we found a geometry relaxation toward a distorted bicapped octahedral structure (most stable when 2S + 1 = 22), which consist of two Rh dimers that are separated by central four Fe atoms in a distorted tetrahedral conformation (Fig. 3, Tables S3-S6). The Rh–Fe–Rh coordination angles are obtuse (larger than 90°), and the Fe–Rh–Fe coordination angles are acute (smaller than 90°). Thus,

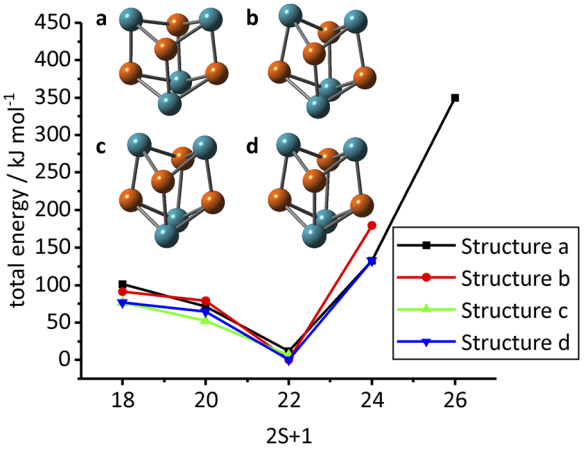

FIG. 3. Total energies of alloy-like $[Rh_4Fe_4]^+$ clusters as a function of the spin multiplicity 2S + 1 relative to the 22tet of structure **(b)**. Structures **(a)–(d)** originate from distinct starting geometries by relaxation in the course of optimization; they converge to a single structural type that comes close to D_{2d} symmetry. Note that only Rh–Fe bonds exist, and the Rh atoms are separated by the Fe atoms (for more details, see the text; Fe: orange and Rh: turquoise).

© Author(s) 2022

the rhodium atoms provide more space for adsorption of N_2. The PW91 functional predicts less Rh–Rh relaxation in distances relative to bulk values than our PBE0 modeling (Table II).

The computed Rh–Rh distances range between 2.706 and 2.737 Å, which is slightly but significantly larger than bond distances in the bulk. Besides likely electron delocalization, the bond length may provide some hints on strength of interaction between the atoms in the cluster. Our computed Rh–Rh and Fe–Fe distances are far off the ones from the dimer data. In the case of structure **(a),** one distance between neighbored Rh atoms (Rh2–Rh3; cf. Table S3) seems much too long to indicate a bond. For $[Rh_4Fe_4]^+$, the Fe–Fe and Rh–Rh distances seem too long for a binding interaction. This would allow for large-scale flexibility at little enthalpic penalty. In contrast, all the computed Rh–Fe distances are short, indicating binding, for sure a stronger interaction than for Rh–Rh and Fe–Fe.

This implies that in the $[Rh_4Fe_4]^+$ cluster, Rh–Fe bonds are dominant and each Rh atom is coordinated by three Fe atoms and vice versa. Moreover, within this $[Rh_4Fe_4]^+$ cluster, the Fe–Fe and Rh–Rh interactions seem diminished in favor of dominant Fe–Rh bonding. This cluster is sufficiently large to maximize the favorable Rh–Fe interactions and to allow for considerable mixing. Structure **(a)** has relaxed to C_{2v}, and it is somewhat less stable (by ~6 kJ/mol) than **(b)**–**(d)**, all of which resume almost perfect D_{2d} symmetry.

B. IR spectroscopy of N_2 adsorption onto $[Rh_iFe_j]^+$ $i = j = 3, \ldots, 8$ clusters

We recorded IR-MPD spectra of N_2 adsorbed onto equiatomic rhodium–iron cluster cations (Figs. 4 and 5), and we found multitudes of bands, which are red shifted with respect to the free N_2 stretching vibration at 2330 cm^{-1}.[65] The obtained band positions range from 2175 to 2315 cm^{-1}. This is to compare to N_2 adsorbate spectra of cobalt clusters (2170–2290 cm^{-1})[15] and to those of nickel (2175–2280 cm^{-1}),[21,22] tantalum (2180–2325 cm^{-1}),[53] iron (2270–2310 cm^{-1}),[43] and rhodium clusters (2180–2270 cm^{-1}).[24] The red and green shaded areas in the present spectra (Figs. 3 and 4) mark the previously found ranges of the band positions of single N_2 when adsorbed to pure rhodium and iron clusters, respectively.

In our present study, we took IR-MPD spectra of equiatomic $[Rh_iFe_j(N_2)_m]^+$ clusters at three values of m: single N_2 adsorption $m = 1$ (black line in Figs. 4 and 5), intermittent coverage state (green shaded areas in Fig. 4), and high numbers of adsorbed N_2 (blue shaded areas in Figs. 4 and 5). For (3,3,m), we recorded IR-MPD spectra of $m = 1$ and 7, omitting the case of intermittent coverage. For exemplary measurements down to below 1200 cm^{-1} and further recorded spectra of some more cluster adsorbate complexes (i,j,m), refer to the supplementary material.

1. The cases of single N_2 adsorption

In the cases of single and intermittent N_2 adsorption (Fig. 4) onto $[Fe_iRh_j]^+$ clusters, we observe vibrational bands around 2250 ± 50 cm^{-1}, which coincides with the range of previously found vibrational bands of pure Rh cluster N_2 adsorbates.[24] This implies red shifts of about 30–130 cm^{-1} with respect to the IR inactive stretching vibration of free N_2 (2330 cm^{-1}).[65] Encouraged by this coincidence, we assume that single N_2 preferentially adsorbs to a rhodium atom rather than to an iron atom. We find support for this assumption from previously calculated adsorption energy of N_2 on rhodium surfaces (54 kJ/mol), which is considerably higher than that on Fe surfaces (34 kJ/mol).[1] Our own calculations on $[Rh_5(N_2)_m]^+$ cluster adsorbate complexes yielded an adsorption energy of 65 kJ/mol for the first adsorbate molecule.[44]

a. $[Rh_3Fe_3(N_2)_1]^+$ *to* $[Rh_5Fe_5(N_2)_1]^+$. In all cases up to $i = j = 5$, there are single strong bands of single N_2 adsorbates ($m = 1$) at 2266, 2253, and 2237 cm^{-1}. These single bands gradually red shift by 29 cm^{-1}. Such a red shift was observed before in the case of N_2 adsorption to pure cobalt and rhodium cluster cations, and it was interpreted in terms of a cooperative polarization effect:[15,24]

TABLE II. Calculated atomic distances (in Å) for nearest neighbors for the $[Rh_4Fe_4]^+$ clusters (22tet) in comparison with the sum of atomic radii, experimental data, and calculations on a bicapped octahedral structure.

	Sums of atomic radii		PW91[a]	PBE0[b]	PBE0[b]	PBE0[b]	PBE0[b]
Species	Dimer	Bulk		**(a)**	**(b)**	**(c)**	**(d)**
Rh–Rh	Theo. 2.21[a] Theo. 2.27[d] Exp. 2.3855[e] Exp. 2.28[f]	2.69[c]	2.70	2.751–3.307	2.715–2.737	2.706–2.716	2.715–2.737
Rh–Fe		2.586[c] 2.581[h]	2.42	2.332–2.412	2.361–2.537	2.375–2.433	2.362–2.715
Fe–Fe	Exp. 2.198(2) –2.2318(8)[g]	αFe 2.482[c]	2.45	2.839–2.842	2.826–2.779	2.615–2.839	2.766–2.827

[a]Reference 41.
[b]This work.
[c]Reference 62. Distance of the next neighbors in the fcc crystal; lattice parameter a = 3.8032 Å.
[d]Reference 58.
[e]Reference 59.
[f]Reference 60.
[g]Reference 61.
[h]Reference 63.

© Author(s) 2022

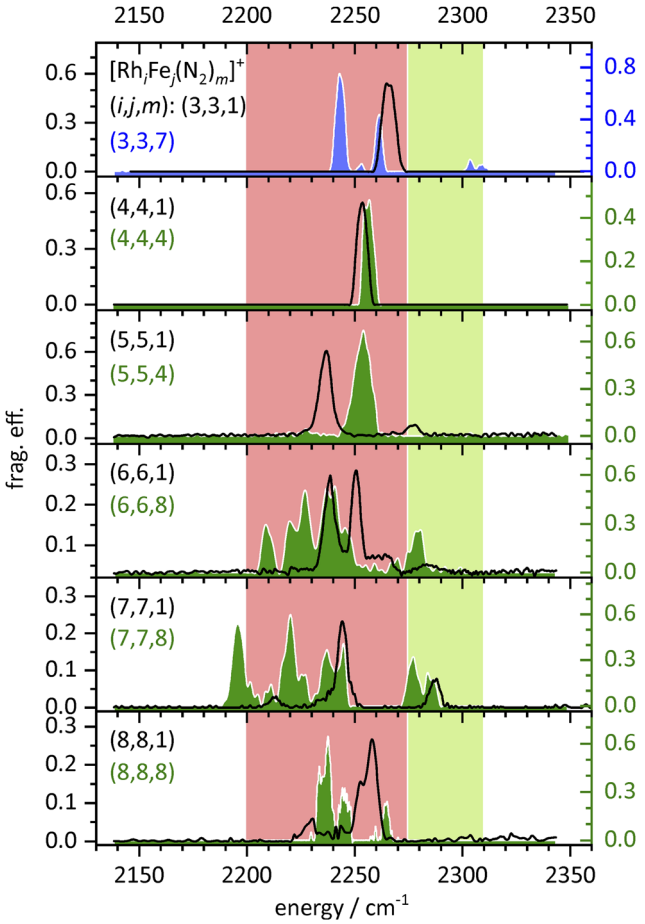

FIG. 4. IR-MPD spectra of single N_2 adsorption (black line) and of first intermittent N_2 adsorption (see the exptl. part; green shaded) on equiatomic alloy cluster cations $[Fe_iRh_j(N_2)_m]^+$ as a function of the size of the cluster core $i = j$. In the case of $i = j = 3$, the blue color denotes the absence of any intermittent adsorption limit. Instead, we provide the spectrum of the maximum N_2 adsorption limit at $m = 7$. The red and green shaded backgrounds indicate the known spectral ranges of the single N_2 vibrations on pure Rh and Fe cluster cations, respectively (for further details, see the text).

the (likely) metallic nature of the cluster cations allows for electron density back donation to molecular adsorbate acceptors (e.g., antibonding π^*). This would weaken the N–N bond and increase the red shift of the N_2 stretching frequency with the number of metal atoms. The further weak IR-MPD band of (5,5,1) at 2277 cm^{-1} likely stems from a combination band of N–N stretching plus Rh–N–N wagging character plus 40 cm^{-1} with respect to the pure N–N stretching band. We calculated an adsorption energy of the first N_2 onto the $Rh_3Fe_3^+$ cluster (cf. Table S7, Fig. S13) as high as 90 kJ/mol.

b. $[Rh_6Fe_6(N_2)_1]^+$. The $i = j = 6$ case is special in revealing two strong IR-MPD bands at 2239 and 2251 cm^{-1} by a mere single N_2 adsorbate, $m = 1$ (black line in Fig. 4). This may likely indicate two distinguishable N_2 binding sites, less likely two cluster isomers, and even less likely two spin state isomers. If, indeed, so, one may tentatively conclude on the presence of Rh atoms in two different coordination geometries, which vary either by the number or by the nature of nearest neighbors. Of course, the presence of coexistence cluster isomers is conceivable as well. Elucidation remains to future DFT modeling. Above the second strong band, we find some more absorption around 2265 and 2285 cm^{-1}. Both may also originate from some combination band of N–N stretching plus Rh–N–N wagging character, the latter contributing by about 25 and 35 cm^{-1}, respectively.

c. $[Rh_7Fe_7(N_2)_1]^+$ *and* $[Rh_8Fe_8(N_2)_1]^+$. When inspecting the IR spectra of these larger clusters, the $m = 1$ cases reveal a remarkable blue shift of the observed single strong N_2 vibrational bands of 5 cm^{-1} from $i = j = 6$ to 7 (2244 cm^{-1}) and of 14 cm^{-1} from $i = j = 7$ to 8 (2258 cm^{-1}). This is surprising at first sight. If we assume an alloy-like structure, that is, only Rh–Fe bonds and no Rh–Rh or Fe–Fe bonds within these clusters, the number of iron atoms coordinating to each Rh atom will increase with the size of the cluster. Since Fe is more electronegative than Rh, more electron density is shifted from Rh to Fe and the vibrational frequency of Rh attached N_2 will decrease, which is due to less π-backbonding. The known charge dilution effect[19] may also contribute to some extent, which would be minor for clusters of this size, however. The (8,8,1) cluster adsorbate complex has an additional shoulder on the red slope of the strong band at 2253 cm^{-1} that may indicate a second N_2 binding site. Both clusters, (7,7,1) and (8,8,1), show an additional band about 30 cm^{-1} to the red of the strong bands at 2213 and 2231 cm^{-1}, respectively. We observed these bands only upon exposure to high IR photon fluxes, and we assume these to represent hot bands. The spectrum (7,7,1) cluster adsorbate complex reveals an additional band red shifted with respect to the free N_2 stretching vibration by only 43 cm^{-1} at 2287 cm^{-1}, which may arise from a combination mode of N–N stretching and Rh–N–N wagging modes as assumed above for the cases of (5,5,1) and (6,6,1).

2. The cases of the "intermittent adsorption limits"

As outlined in Sec. II, we have defined those cluster adsorbate complexes as an intermittent adsorption limit where we find enhanced amounts of N_2 adsorption and delayed kinetics for further adsorption. Note that in all the investigated cases of $i = j = 4, ..., 8$, there are such intermittent adsorption limits—but for the smallest cluster case, $i = j = 3$, where N_2 adsorption proceeds toward its maximum limit without any intermittent delay.

a. $[Rh_3Fe_3(N_2)_7]^+$. We observe two strong bands (at 2243 and 2261 cm^{-1}), one weak band (in between at 2253 cm^{-1}), and a couple of very weak near coinciding bands around 2305 cm^{-1} [blue spectrum, indicated as (3,3,7), in Fig. 4]. The former three of these bands fall within the red shaded area, and they likely stem from the stretching vibrations of those N_2 adsorbates, which adsorb onto Rh sites. The super-stoichiometric composition of a 6:7 metal:adsorbate ratio requires at least one metal site with geminal N_2 adsorption. We assume a monolayer with single adsorption of the first six N_2 molecules onto the $[Rh_3Fe_3]^+$ cluster, and the seventh N_2 adsorbs onto an already singly occupied site.

Symmetric/asymmetric couplings of those equivalent N_2 oscillators are expected to induce significant splittings. Further insights will arise from the DFT modeling of such vibrations (refer to chapter/section III C). The weak bands around 2305 cm^{-1} fall into the green shaded area of Fe–N_2 stretching vibrations, and they likely

© Author(s) 2022

arise from such N_2 adsorptions to iron sites. Note that this IR-MPD spectrum does not provide any discernible evidence for isomerization of any type, which well coincides with the swift adsorption kinetics up to the maximum adsorption limit as reported in **[AAE]**.[42]

b. $[Rh_4Fe_4(N_2)_4]^+$. This cluster shows a single band at 2257 cm^{-1}, slightly blue shifted with respect to single N_2 adsorption by about 4 cm^{-1}, and well within the red shaded area of N_2 adsorption to Rh sites. This occurrence of a single band by numerous IR active N_2 oscillators is indicative of a high cluster symmetry. The computations of $[Rh_4Fe_4]^+$ structures have suggested such a high symmetry in a D_{2d}-like structure (cf. inset of Fig. 5). All Rh atoms and all Fe atoms have the same coordination geometry, respectively; all Rh sites and all Fe sites are equivalent, respectively. An exclusive N_2 adsorption to Rh sites finds further support by structural and enthalpic reasons: The Rh atoms are coordinated by Fe with acute Fe–Rh–Fe angles, and they protrude from the cluster surface.

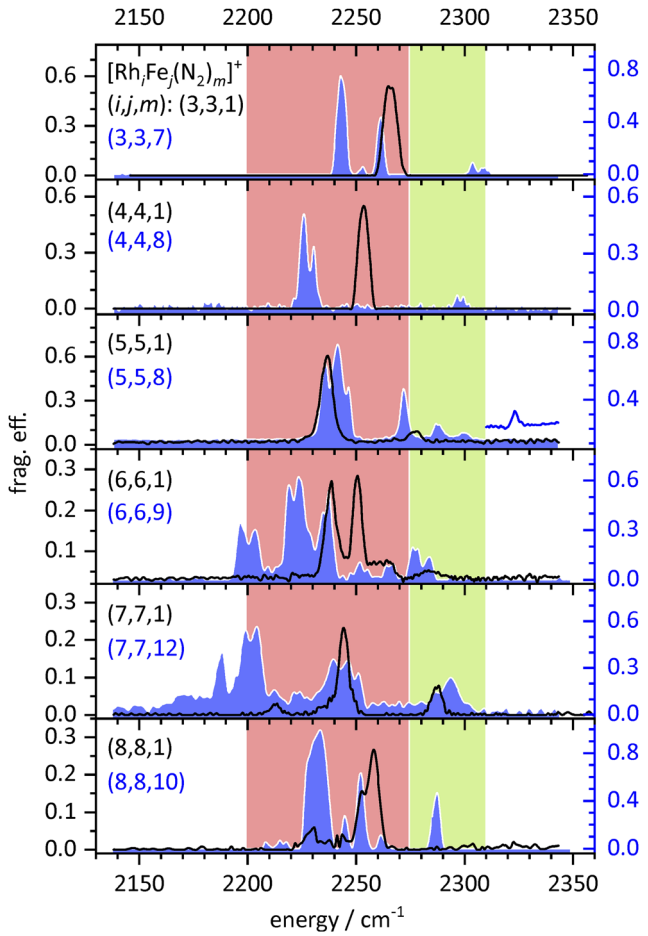

FIG. 5. IR-MPD spectra of single (black line) and high N_2 adsorption (blue shaded) on equiatomic cationic Rh–Fe alloy cluster cations as a function of the size of the cluster core $i = j$. The red and green shaded backgrounds indicate the known spectral ranges of the single N_2 vibrations on pure Rh and Fe cluster cations, respectively (for details, see the text).

This reduces steric hindrance by next neighbors and provides open space. For Fe sites, the opposite holds. Enthalpic reasoning arises from the computed N_2 adsorption enthalpies of pure Fe and Rh surfaces—which are stronger for Rh than for Fe.[1]

c. $[Rh_5Fe_5(N_2)_4]^+$. The IR-MPD spectrum of this cluster shows a single band at 2254 cm^{-1}, which falls into the red area, and it almost coincides with the single band of the $[Rh_4Fe_4(N_2)_4]^+$ cluster adsorbate complex. Note the difference to the (4,4,1) and (5,5,1) cases, where the two single bands are displaced against each other by about 17 cm^{-1}. Once more, we take the occurrence of a single absorption band by multiple N_2 adsorbates as strong evidence for a cluster structure of high symmetry. However, its very nature is yet unexplored. A very weak band at 2227 cm^{-1} might indicate either a hot band or a second isomer. Supporting DFT calculations are beyond the scope of the present study.

d. $[Rh_6Fe_6(N_2)_8]^+$ *and* $[Rh_7Fe_7(N_2)_8]^+$. In contrast to the IR-MPD spectra of the smaller clusters, these clusters provide spectra with numerous bands within the red shaded area of N_2 adsorption to Rh sites; they spread out over a range of up to 75 cm^{-1}. This likely points out that the Rh coordination sites are distinguishable and that these clusters are of low symmetry. There are bands at 2209, 2220, 2227, 2237, 2241, and 2245 cm^{-1} of the (6,6,8) cluster adsorbate complex and at 2175, 2210, 2220, 2226, 2237, and 2244 cm^{-1} of the (7,7,8) cluster adsorbate complex. There are some additional bands in the range of 2270–2290 cm^{-1} that fall into the green shaded area of likely N_2 adsorption to Fe sites. Such adsorption is, indeed, conceivable in cases where the number of N_2 adsorbates exceeds the adsorbing Rh sites within the cluster. The excess of N_2 molecules may choose to accept the less favorable Fe sites. Of course, it is conceivable to adsorb multiple N_2 to single Rh, which might induce further splittings by symmetric/asymmetric coupling. Given the high total number of metal atoms in these clusters (12 and 14, respectively), it is likely that some atoms are not at the cluster surface. They may assume high coordination to the inside and form bulk-like bonding motifs. This remains to verify.

e. $[Rh_8Fe_8(N_2)_8]^+$. In this intermittent adsorption limit case, the number of adsorbed N_2 molecules is the same as the number of Rh and Fe atoms, each. The IR-MPD spectrum reveals several bands within the red shaded area of preferential N_2 adsorption to Rh sites (at 2233, 2238, 2245, and 2265 cm^{-1}); there are no bands in the range of single Fe–N_2 adsorption. In view of the previous findings, all N_2 molecules seem to adsorb to Rh sites only—albeit to distinguishable ones. We observe two weak bands about +20 cm^{-1} to blue, which we tentatively assign to stretch/wag combinations. All of this indicates a cluster structure of some symmetry that is slightly distorted. These findings may serve as a valuable starting point for further elucidation by future DFT modeling.

3. The cases of "maximum adsorption limits"

We recorded IR-MPD spectra of highly abundant clusters with high N_2 coverages, (4,4,8), (6,6,9), and (8,8,10), and of maximum adsorption limits (5,5,8) and (7,7,12). For all of these cluster adsorbate complexes, $m > i$. The (3,3,7) case is discussed above.

a. $[Rh_4Fe_4(N_2)_8]^+$. Despite the high level of N_2 adsorption, $m = 8$, we observe a single band at 2226 cm^{-1} with a shoulder at 2231 cm^{-1}. The center of this double band is red shifted by 25 cm^{-1}

© Author(s) 2022

with respect to single N_2 adsorption, $m = 1$, and by 28 cm^{-1} with respect to the intermittent N_2 adsorption, $m = 4$. By virtue of the red and green shaded areas, all the N_2 molecules likely adsorb onto Rh sites. This is conceivable based on the structural and enthalpic reasons discussed above. Closer inspection of the observed band reveals a small splitting of about 5 cm^{-1}. This likely results from the symmetric/antisymmetric coupling of stretching vibrations of two N_2 on the same Rh site. A weak band around 2297 cm^{-1} likely arises from some N_2 adsorption to Fe sites. Some splitting on the order of 4 cm^{-1} is discernible but close to the noise level. Note that higher levels of N_2 coverage up to $m_{max} = 11$ are in equilibrium, but their abundances are almost 2 orders of magnitude lower than that of $m = 8$.[42] We find no indication of isomerization or swift adsorption/desorption equilibria in the recorded IR-MPD spectra of (4,4,*m*).

b. $[Rh_5Fe_5(N_2)_8]^+$. The strong band of the (5,5,8) cluster at 2241 cm^{-1} appears blue shifted by 4 cm^{-1} from the corresponding band of the (5,5,1) cluster at 2237 cm^{-1} and reveals some triple splitting by 4–6 cm^{-1}. There is an additional set of three weaker bands to the blue at 2272 cm^{-1} and above. We tentatively assign these to other N_2 adsorption sites. The two bands at 2288 and 2299 cm^{-1} are in the green area of N_2 adsorbed likely to Fe clusters.

We may note in passing that in both cases of $i = j = 4$ and 5, the investigated levels of N_2 adsorption are $m = 4$ and $m = 8$. Both IR-MPD bands of $m = 4$ occur around 2254–2257 cm^{-1}, and both IR-MPD bands of $m = 8$ shift considerably to red (12–32 cm^{-1}). Despite these similarities, the single N_2 adsorption cases (4,4,1) and (5,5,1) are remarkably different: The found single IR-MPD bands of $i = j = 4$ and 5 are shifted with respect to each other by 17 cm^{-1}.

There is an additional band at 2323 cm^{-1} that appears only upon application of maximum laser power (2.5 mJ/pulse as opposed to 1 mJ/pulse else). It likely originates from a merely bound and weakly polarized N_2 molecule, roaming around or locating close to other strongly bound N_2 adsorbates. The adsorption rates continuously decrease toward $m_{max} = 8$ (cf. **[AAE]**) and support such a weak interaction of the last N_2 ligand with the cluster.[42] Thus, there may be, indeed, a loosely bound second shell N_2 adsorbate. For all of the least red shifted bands, 2299 cm^{-1} and above, we need to keep in mind the general possibility of stretching wagging combination modes.

c. $[Rh_6Fe_6(N_2)_9]^+$ *and* $[Rh_7Fe_7(N_2)_{12}]^+$ *and* $[Rh_8Fe_8(N_2)_{10}]^+$. In these three cases of $i = j = 6$, 7, and 8, we recorded the IR-MPD spectra of the cluster adsorbate complexes with $m = 9$, 12, and 10, respectively. We found bands for (6,6,9) at 2196, 2203, 2219, 2223, 2237, 2251, 2265, 2276, and 2284 cm^{-1} and for (8,8,10) at 2233, 2245, 2252, 2261, and 2287 cm^{-1}. The bands of the (7,7,12) spectrum separate into two sets: one in the red shaded Rh range at 2188, 2199, 2204, 2213, 2223, 2240, 2247, and 2251 cm^{-1} and one weaker set of overlapping bands in the green shaded Fe range around 2294 cm^{-1}. The spectra closely resemble to those of the lower coverage intermittent adsorption limits discussed above. All spectral features prevail, with some minor shifts and intensity variations occurring. There is one remarkable exception: In the $i = j = 8$ cases, there is an additional band at 2287 cm^{-1} in the $m = 10$ spectrum, which does not show in the $m = 8$ spectrum. This additional band is indicative of N_2 adsorption to Fe sites; it falls into the green shaded spectral area. Thus, we find evidence that the $i = j = 8$ cluster $[Rh_8Fe_8]^+$ adsorbs up to eight N_2 to Rh sites, and two more N_2 adsorbates onto Fe sites thereafter. In all three cases, we did not observe any bands around 2330 cm^{-1}.

With (7,7,12), we were able to record an IR-MPD spectrum of a maximum adsorption limit, despite an adsorption/desorption equilibrium between four species at long storage times.[42] The spectrum shows broad bands, which are in line with a flexible adsorbate shell. The recorded bands exhibit narrow splittings of 4–10 cm^{-1}, which indicate couplings as expected for double N_2 occupation of metal sites.

In addition, we recorded the spectrum of the (7,7,10) intermittent adsorption limit (cf. Fig. S11 of the supplementary material), which reveals remarkably sharp and widely spaced bands—void of the above-mentioned small couplings.

Upon closer inspection, some of the properties of the (6,6,9) and the (7,7,12) spectra warrant some more attention: First, for (6,6,9), the three strongest bands reveal a splitting up to 7 cm^{-1}, which does not show up to the first intermittent N_2 adsorption. Such splittings are likely indicative of symmetric/antisymmetric couplings of two N_2 at the same Rh site; see above. In this case, they show only at high N_2 loads. Even the weak bands in the green shaded area reveal a splitting. We conclude on some Rh and Fe atoms that are more exposed and others that are higher coordinated and thus do adsorb at most single N_2. Second, the (6,6,9) and (7,7,12) spectra spread out over a range of up to 120 cm^{-1}. We assume that the most red shifted bands arise from N_2 adsorption onto a class of Rh atoms that provide a weak σ-acceptor and strong π-donor character. The less red shifted bands arise from N_2 adsorbed onto a class of Rh atoms with a strong σ-acceptor and weak π-donor character. In the case of the (8,8,10) cluster adsorbate complex, these separate classes seem to vanish.

The IR-MPD spectra of (6,6,9) and (8,8,10) document intermittent species, which are in equilibrium with the maximum adsorption limit and which constitute the most abundant species within these equilibria[42] **[AAE]**. In both cases, the adsorption rate constants drop continuously with the increasing number of adsorbed N_2 molecules and the adsorption becomes slower, step by step. Investigation of their true maximum adsorption limits would also probably show weakly bound and weakly activated N_2 ligands as revealed for (5,5,8). However, the low abundance of these maximum adsorption limits (6,6,10) and (8,8,11) and their involvement in swift adsorption/desorption equilibria have impeded their spectroscopic investigation so far.

Quantum chemical modeling of all investigated species and their recorded spectra is far out of reach. Instead, we chose one case of limited complexity for exemplary DFT modeling in order to achieve some better understanding of the adsorption behavior and the structural properties of such an alloy cluster.

C. Modeling of the $[Rh_3Fe_3(N_2)_7]^+$ vibrational spectra

We chose the case of the maximum N_2 adsorption limit of $m_{max} = 7$ to the $i = j = 3$ alloy cluster as a test case for vibrational analysis by further DFT modeling. The most stable (3,3,7) isomers are based on a metal cluster core (3,3,0) of most stable type (**al**). Each of the Rh and Fe sites serves to adsorb single N_2, and the seventh remaining N_2 serves to locate as a second adsorbate on one of the four optional and distinguishable sites (cf. Fig. 6 for atom labeling): at the Rh site

© Author(s) 2022

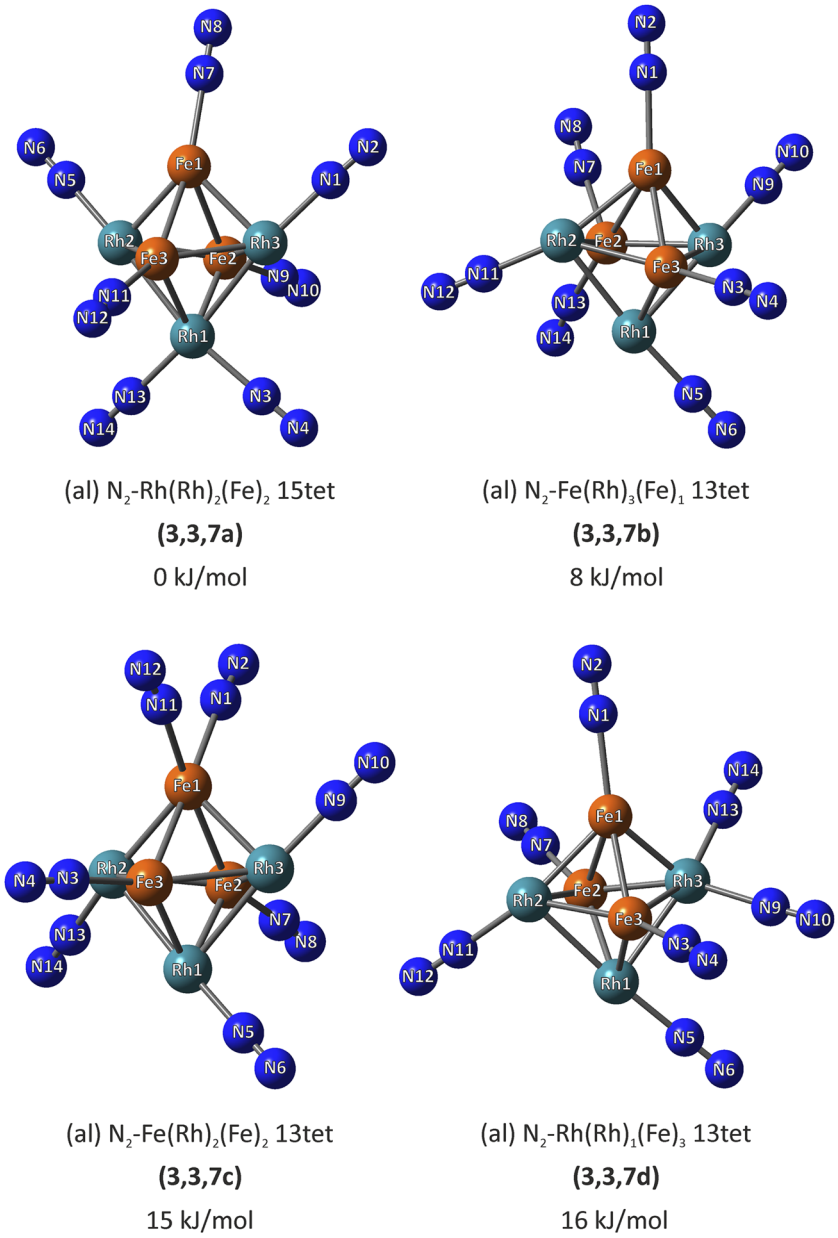

FIG. 6. DFT optimized structures of four most stable $[Rh_3Fe_3(N_2)_7]^+$ clusters. All four isomers derive from the cluster core type (**al**). All N_2s chose to adsorb by μ_1-type end-on coordination. The most stable case **(3,3,7a)** reveals single N_2 adsorbates at each Rh and Fe site, but Rh_1 reveals two geminal N_2 adsorbates. This Rh site is unique by its two Rh next neighbors. Cases **(3,3,7b)** and **(3,3,7c)** reveal two geminal N_2 adsorbates at sites Fe_2 and Fe_1, respectively. Case **(3,3,7d)** reveals geminal N_2 adsorbates at site Rh_3. The xyz coordinates are provided in the supplementary material (Tables S9–S12).

(two Rh next neighbors, labeled Rh_1), at either of two equivalent Rh sites (one Rh next neighbor, labeled Rh_2 and Rh_3), at the Fe site (two Fe next neighbors, labeled Fe_1), or at either of the two equivalent Fe sites (one Fe next neighbor, labeled Fe_2 and Fe_3).

We compare the recorded IR-MPD spectra to our computed IR absorption spectra, where the computed spectra are scaled by 0.9385[24] to match experimental and calculated fundamentals of free N_2 (Fig. 7). It shows that the experimental IR-MPD spectrum matches best to the calculated absorption spectrum of the cluster in a 15tet with the seventh N_2 adsorbed to the sole Rh site with two Rh next neighbors (structures as displayed in Fig. 6; spectrum as in Fig. 7, second to the top). We provide a compilation of assigned vibrational bands in Table III. Note that the calculated and observed bands are slightly shifted in their frequency against each other. However, the overall pattern and the IR intensities agree remarkably well when considering the most stable case of the DFT modeling. The other calculated isomers are at least 46 kJ/mol higher in energy, and their spectra are documented in Fig. S14.

The twofold occupation of a Rh site causes a symmetric/antisymmetric coupling and allows for an assignment of the recorded bands at 2253 cm^{-1} (antisymmetric) and 2261 cm^{-1} (symmetric) (N_3/N_4 and N_{13}/N_{14}). It is remarkable that there is a

© Author(s) 2022

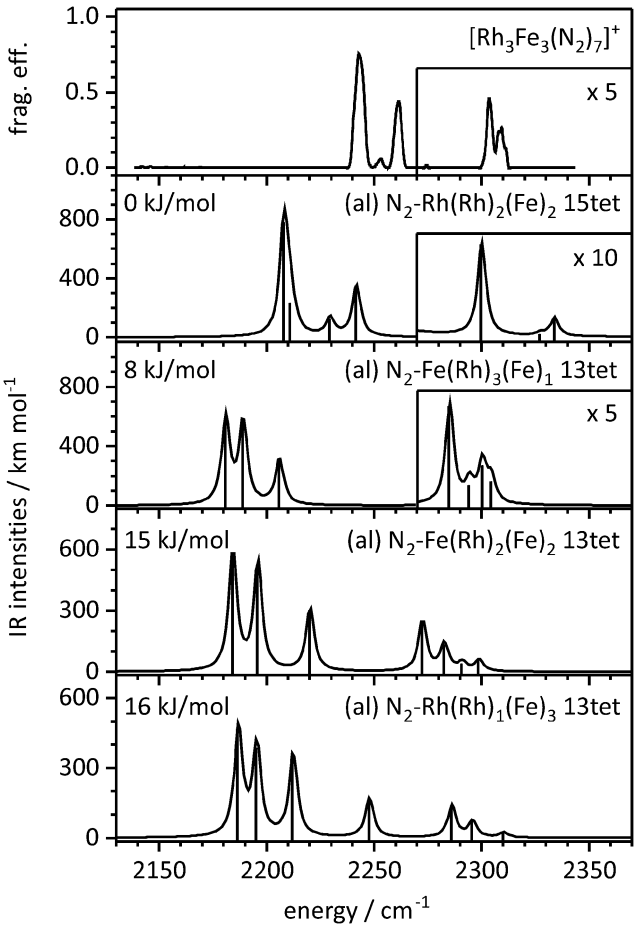

FIG. 7. Experimental IR-MPD spectrum (top trace) and calculated IR absorption spectra of some $[Rh_3Fe_3(N_2)_7]^+$ coordination and spin isomers. The calculated spectra (scaled by 0.9385) represent the four preferential coordination and spin isomers from Fig. 6. Note the slightly shifted and otherwise matching pattern of vibrational modes in the topmost computed spectrum of the most stable isomer **(3,3,7a)**, which comes along in a 15tet spin state.

significant shift between the bands of N_2 adsorbed on Fe and on Rh. Indeed, all bands around 2250 cm^{-1} can be assigned to stretching vibrations of N_2 on rhodium—in line with our working hypothesis that spectral findings from pure Rh and pure Fe clusters may serve as a guide for a classification of spectral feature in the mixed alloy-type Rh–Fe clusters (visualized by the red and green shaded areas in Figs. 4 and 5).

The calculations indicate a symmetric/antisymmetric N_2–Rh–Rh–Rh–N_2 coupling between the stretching vibrations of N_1/N_2 and N_5/N_6. The coupling of these two distant but equivalent N_2 ligands is very weak (calculated as 3–4 cm^{-1}) and does not necessarily manifest in separate bands. The weak recorded bands above 2300 cm^{-1} can be assigned to N_2 adsorbed to Fe. Calculations indicate no vibrational coupling between these Fe bound N_2 adsorbates. The calculated IR spectra of less stable coordination isomers (the two lower traces in Fig. 7) do not fit to the experimental IR-MPD spectrum. These results are in line with our kinetic measurements that exhibit swift adsorption to a single maximum adsorption limit without any equilibrium at the end of the adsorption chain.[42]

In (3,3,7), the first six N_2 molecules adsorb onto a free metal site such that each metal site is singly occupied, independent of the metal (Rh or Fe). We observe a Langmuir type of stoichiometric adsorption. The seventh N_2 molecule has no choice but to adsorb onto an occupied site and finds itself as a geminal adsorbate, preferentially at a Rh site. The adsorption kinetics reveal a swift stepwise adsorption without any indication of an intermittent adsorption limit.[42] The IR bands of the N_2 molecules adsorbed onto the Rh sites are in the range as observed for pure Rh clusters; those of N_2 adsorbed onto Fe sites are in the range as observed for pure Fe clusters, and these IR bands are by at least one order of magnitude less intense than the N_2 stretching IR bands at Rh sites. The polarization of N_2 by adsorption to Fe sites seems weaker than that by adsorption to Rh sites. Note that these results indicate a conservation of the 15tet spin state at the maximum adsorption limit (3,3,7) rather than a spin quench as observed for pure rhodium clusters before.[24,44]

The modeling of the (3,3,7) cluster adsorbate complex, the thereby achieved assignment of recorded IR bands, and fur-

TABLE III. Vibrational data for the lowest lying $[Rh_3Fe_3(N_2)_7]^+$ structure. The scaling factor for the N_2 stretching frequencies is 0.9385. The low frequency modes are strongly coupling.

Mode	Type	Calc. freq. (cm^{-1})	Scaled freq. (cm^{-1})	IR intensity (km mol^{-1})	Measured $\tilde{\nu}$ (cm^{-1})
1–18	Wagging modes	9.3–77	8.7–72	0.009–11	
19–32	Internal cluster vibrations	99–231	93–217	0.044–5.3	
33–47	Bending modes	249–343	234–322	0.39–32	
48	Asymm. stretch N_1–N_2/N_5–N_6	2352	2207	778	2243
49	Symm. stretch N_1–N_2/N_5–N_6	2356	2211	233	
50	Asymm. stretch N_3–N_4/N_{13}–N_{14}	2375	2229	124	2253
51	Symm. stretch N_3–N_4/N_{13}–N_{14}	2388	2241	351	2261
52	Stretch N_7–N_8	2450	2299	63	2304
53	Stretch N_{11}–N_{14}	2479	2327	2.3	2309
54	Stretch N_9–N_{10}	2487	2334	13	

© Author(s) 2022

ther insights above support in the interpretation of the (4,4,8) spectrum.

The IR-MPD spectrum of the (4,4,8) cluster adsorbate complex reveals a strong doublet band in the Rh range and a weak set of bands in the Fe range. Such a sparse spectrum by eight chromophores strongly suggests a single type of Rh adsorption sites and of Fe adsorption sites, which implies high symmetry. The recorded band in the Rh range is split by about 4 cm^{-1}, which likely indicates symmetric/antisymmetric coupling of a distant pair of N_2 molecules whose adsorption sites are separated by another metal atom, as revealed in the (3,3,7) case above. In the IR-MPD spectrum of (4,4,8), there is no indication of a splitting in the order of 12 cm^{-1} and therefore no indication for double adsorption onto a single metal site. The IR-MPD spectrum thus indicates stoichiometric adsorption onto each of the eight metal sites. The IR-MPD spectrum of the (4,4,4) cluster adsorbate complex has not revealed any evidence for N_2 occupation of Fe sites, and the recorded single band indicates a highly symmetric cluster. The adsorption kinetics reveal an intermittent adsorption limit for this complex. We conclude on a highly symmetric cluster core that likely resembles the computed most stable D_{2d} structural type. The first four N_2 molecules likely adsorb onto the equivalent Rh atoms, whereas the remaining four adsorption steps yield at the equivalent Fe sites. The final product is a highly symmetric cluster adsorbate complex (4,4,8) with a Langmuir-type stoichiometric first adsorption shell.

IV. CONCLUSION

We have recorded IR-MPD spectra of size selected N_2 adsorbates on equiatomic Rh–Fe cluster cations. These spectra show a multitude of bands within ranges that coincide with spectra of N_2 adsorbates on Rh and Fe cluster cations recorded before. The sparse spectra of the cluster adsorbate complexes of $[Rh_4Fe_4]^+$ and $[Rh_5Fe_5]^+$ indicate high symmetries of these.

We have modeled geometries of $[Rh_3Fe_3]^+$ and $[Rh_4Fe_4]^+$ clusters and IR spectra of the $[Rh_3Fe_3(N_2)_7]^+$ cluster, which confirm the propensity of the clusters to form as much Rh–Fe bonds as possible and which allow for high symmetry and an alloy-like character. A comparison with our adsorption kinetics yields a conclusive description of spectral phenomena, such as weakly adsorbed N_2 ligands. By the assignment of the blue shifted bands to Fe adsorption sites, we validate the sensitivity of the element of the N_2 stretching vibration with respect to adsorption to Fe or Rh sites. In the case of the $[Rh_3Fe_3]^+$ cluster, we conclude on the formation of an N_2 monolayer on all metal atoms. The next N_2 molecule adsorbs onto a Rh atom in a geminal manner. The spectrum of the $[Rh_4Fe_4]^+$ cluster indicates an adsorption of the first four N_2 molecules solely/exclusively onto the rhodium atoms. The spectrum of $[Rh_4Fe_4(N_2)_8]^+$ indicates additional stoichiometric adsorption onto iron atoms. In contrast to bare rhodium clusters, our investigations do not provide any indication for a spin quench upon N_2 adsorption.

The present IR-MPD studies in conjunction with the DFT modeling relate recorded IR bands to element specific adsorption sites. We thereby find strong evidence for preferential adsorption to rhodium sites and merely secondary adsorption to iron.

SUPPLEMENTARY MATERIAL

See the supplementary material for spectral IR photon fluxes, for structural parameters and plots of computed cluster isomers, and for further IR-MPD spectra of further cluster adsorbate complexes.

ACKNOWLEDGMENTS

This work was supported by the German Research Foundation (DFG) within the Transregional Collaborative Research Center SFB/TRR 88 "Cooperative effects in homo- and heterometallic complexes" (3MET.de) and by the State Research Center OPTIMAS. We thank Thomas Kolling for assistance on technical questions of any kind. Finally, we thank the reviewers for most valuable comments, which are much appreciated.

AUTHOR DECLARATIONS

Conflict of Interest

The authors have no conflicts to disclose.

Author Contributions

M.P.K., A.A.E., M.E.H., A.S., D.V.F., S.D., and J.M. conducted the experiments. A.A.E. and M.P.K. carried out quantum chemical calculations. M.P.K. and G.N.-S. evaluated all data. M.P.K., S.D., and G.N.-S. wrote the manuscript, and all the authors revised and agreed.

DATA AVAILABILITY

The data that support the findings of this study are available from the corresponding author upon reasonable request.

REFERENCES

[1] T. Bligaard and J. K. Nørskov, *Chemical Bonding at Surfaces and Interfaces* (Elsevier, Amsterdam, 2008), p. 255.
[2] G. A. Somorjai, *Introduction to Surface Chemistry and Catalysis* (John Wiley & Sons, 1994),
[3] O. Deutschmann *et al.*, *Ullmann's Encyclopedia of Industrial Chemistry* (Wiley-VCH Verlag GmbH & Co. KGaA, 2000).
[4] M. Votsmeier *et al.*, *Ullmann's Encyclopedia of Industrial Chemistry* (Wiley-VCH Verlag GmbH & Co. KGaA, 2009).
[5] G. Ertl, Angew. Chem., Int. Ed. **47**, 3524 (2008).
[6] B. Harrison, B. J. Cooper, and A. J. J. Wilkins, Platinum Met. Rev. **25**, 14 (1981).
[7] G. Ertl, Catal. Rev. **21**, 201 (1980).
[8] S. Brunauer, P. H. Emmett, and E. Teller, J. Am. Chem. Soc. **60**, 309 (1938).
[9] I. Langmuir, J. Am. Chem. Soc. **40**, 1361 (1918).
[10] H.-J. Freund *et al.*, Surf. Sci. **185**, 187 (1987).
[11] H. P. Wang and J. T. Yates, J. Phys. Chem. **88**, 852 (1984).
[12] D. A. J. M. Ligthart *et al.*, Catal. Commun. **77**, 5 (2016).
[13] D. E. Jaramillo *et al.*, Nat. Mater. **19**, 517 (2020).
[14] C. Kerpal *et al.*, J. Phys. Chem. C **117**, 12153 (2013).
[15] S. Dillinger *et al.*, Phys. Chem. Chem. Phys. **17**, 10358 (2015).
[16] G. Blyholder, J. Phys. Chem. **68**, 2772 (1964).
[17] J. Chatt and L. A. Duncanson, J. Chem. Soc. **1953**, 2939.
[18] J. S. Dewar, Bull. Soc. Chim. Fr. **18**, C71 (1951).
[19] A. Fielicke *et al.*, J. Chem. Phys. **124**, 194305 (2006).
[20] A. D. Brathwaite, H. L. Abbott-Lyon, and M. A. Duncan, J. Phys. Chem. A **120**, 7659 (2016).

© Author(s) 2022

[21] J. Mohrbach, S. Dillinger, and G. Niedner-Schatteburg, J. Phys. Chem. C **121**, 10907 (2017).
[22] S. Dillinger, J. Mohrbach, and G. Niedner-Schatteburg, J. Chem. Phys. **147**, 184305 (2017).
[23] S. Dillinger *et al.*, J. Phys. Chem. Lett. **9**, 914 (2018).
[24] M. P. Klein *et al.*, Top. Catal. **61**, 106 (2018).
[25] J. Mohrbach, S. Dillinger, and G. Niedner-Schatteburg, J. Chem. Phys. **147**, 184304 (2017).
[26] A. Nilsson, L. G. M. Pettersson, and J. K. Nørskov, *Chemical Bonding at Surfaces and Interfaces*, 1st ed. (Elsevier, Amsterdam; Boston, MA, 2008).
[27] C. Paduani, J. Appl. Phys. **90**, 6251 (2001).
[28] A. Hernando *et al.*, Mater. Sci. Forum **235–238**, 675 (1997).
[29] A. Kashyap *et al.*, J. Appl. Phys. **95**, 7480 (2004).
[30] R. Y. Gu and V. P. Antropov, Phys. Rev. B **72**, 012403 (2005).
[31] W. Lu *et al.*, J. Mater. Sci. **45**, 4919 (2010).
[32] K. Ohtake *et al.*, IEEE Trans. Magn. **50**, 1 (2014).
[33] X. Marti *et al.*, Nat. Mater. **13**, 367 (2014).
[34] A. Heidarian *et al.*, Nucl. Instrum. Methods Phys. Res., Sect. B **358**, 251 (2015).
[35] Y. Wakisaka *et al.*, Phys. Rev. B **92**, 184408 (2015).
[36] J. Clarkson *et al.*, Scientific Reports **7**, 15460 (2017).
[37] D. Odkhuu, Phys. Rev. B **93**, 064412 (2016).
[38] R. Witte *et al.*, Phys. Rev. B **93**, 104416 (2016).
[39] J. Chaboy *et al.*, Phys. Rev. B **59**, 3306 (1999).
[40] J. H. Mokkath and G. M. Pastor, Phys. Rev. B **85**, 054407 (2012).
[41] J. H. Mokkath and G. M. Pastor, J. Phys. Chem. C **116**, 17228 (2012).
[42] A. A. Ehrhard *et al.*, "Cryo Kinetics of N_2 Adsorption onto Bimetallic Rhodium-Iron Clusters in Isolation," J. Chem. Phys. (in press).
[43] A. Straßner *et al.*, J. Chem. Phys. **155**, 244305 (2021).
[44] A. A. Ehrhard *et al.*, Mol. Phys. **119**, e1953172 (2021).
[45] P. Caravatti and M. Allemann, Org. Mass Spectrom. **26**, 514 (1991).
[46] M. Gerhards, Opt. Commun. **241**, 493 (2004).
[47] M. Grunze *et al.*, Phys. Rev. Lett. **53**, 850 (1984).
[48] M. C. Tsai *et al.*, Surf. Sci. **155**, 387 (1985).
[49] L. J. Whitman *et al.*, Phys. Rev. Lett. **56**, 1984 (1986).
[50] L. J. Whitman, C. E. Bartosch, and W. Ho, J. Chem. Phys. **85**, 3688 (1986).
[51] C. N. R. Rao *et al.*, Spectrochim. Acta, Part A **43**, 1479 (1987).
[52] P. Rochana, K. Lee, and J. Wilcox, J. Phys. Chem. C **118**, 4238 (2014).
[53] D. V. Fries *et al.*, Phys. Chem. Chem. Phys. **23**, 11345 (2021).
[54] M. J. Frisch *et al.*, Gaussian 09, Revision D.01 (Gaussian, Inc., Wallingford, CT, 2009).
[55] C. Adamo and V. Barone, J. Chem. Phys. **110**, 6158 (1999).
[56] T. H. Dunning, J. Chem. Phys. **90**, 1007 (1989).
[57] D. Andrae *et al.*, Theor. Chim. Acta **77**, 123 (1990).
[58] M. R. Beltran *et al.*, Eur. Phys. J. D **67**, 63 (2013).
[59] F. A. Cotton *et al.*, Acta Crystallogr., Sect. B: Struct. Sci., Cryst. Eng. Mater. **27**, 1664 (1971).
[60] K. A. Gingerich and D. L. Cocke, J. Chem. Soc., Chem. Commun. **1972**, 536.
[61] C. A. Murillo, Angew. Chem., Int. Ed. **48**, 5076 (2009).
[62] D. R. Lide and D. M. Haynes *CRC Handbook of Chemistry and Physics*, 90th ed. (CRC Press, Boca Raton, 2010).
[63] A. I. Zakharov *et al.*, J. Exp. Theor. Phys. **19**, 1348 (1964).
[64] D. J. Harding *et al.*, J. Chem. Phys. **133**, 214304 (2010).
[65] J. Bendtsen, J. Raman Spectrosc. **2**, 133 (1974).

© Author(s) 2022